Pergamon

Phys. Chem. Earth, Vol. 22, No. 1–2, pp. 63–68, 1997

Printed in Great Britain
0079-1946/97 $17.00 + 0.00

PII: S0079-1946(97)00078-5

Damage of Saturated Rocks Undergoing Triaxial Deformation Using Complex Electrical Conductivity Measurements: Mechanical Modelling

J. B. Gómez, P. W. J. Glover and P. G. Meredith

Rock and Ice Physics Laboratory, Research School for Geological and Geophysical Sciences, University College London, Gower St., London WC1E 6BT, U.K.

Received 12 June 1996; accepted 12 June 1997

Abstract. Measurements of complex electrical conductivity as a function of frequency is an extremely sensitive probe for changes in pore and crack volume, crack connectivity, and crack surface topography. Such measurements have been made during triaxial deformation experiments on rock samples, at varying confining pressures. The first part of this paper [Glover et al., 1996, this volume] described the effects of triaxial deformation on the complex electrical conductivity of saturated porous rocks. This second part will use these measurements to model the mechanical stress-strain behavior of porous rocks by deriving first a crack damage parameter from the complex electrical conductivity data at a frequency of 1 kHz. The electrical conductivity-derived crack damage parameter is then used as an input to a model of cracked solid, and inverted to reconstruct the experimental stress-strain curves. The resultant synthetic stress-strain curves show good agreement with the experimentally derived stress-strain curves, and the values of the parameters after the inversion procedure compare succesfully with the experimenatally-derived ones.

1 Introduction

The failure of brittle materials during compression is preceded by the formation, growth and coalescence of microcracks [Atkinson, 1987, Lawn, 1993]. This process of accumulated microcracking, termed *damage*, produces a concommitant change in bulk elastic properties, and the goal of a damage model is to predict changes in elastic properties from changes in the crack population. The geometrical properties of the crack population are lumped into a scalar or tensorial *crack damage parameter*, (CDP also termed crack density parameter in the literature of cracked solids), which accounts for basic properties of individual microcracks as size, aspect ratio, and orientation, and also for properties of the crack population as spatial distribution. The most commonly used CDP is defined in three dimensions as [Kachanov, 1992]:

$$\chi = \frac{4}{3}\frac{\pi}{V}\sum_{i=1}^{n_f} l_i^3 , \tag{1}$$

where l_i is the mayor semiaxis of the ith crack (out of n_f) inside volume V. If crack length is independent of orientation, the previous expression can be rewritten as $\chi = n_f \bar{l}^3/V$, which means that crack density is a measure of the relative volume of spheres with cracks as diameters. It is important to note that crack density and crack porosity (i.e., the standard experimental measure of the volume accupied by cracks relative to bulk volume) are not equivalent quantities. For n_f three dimensional spheroidal cracks of aspect ratio $r = c/l$ inside volume V (c being the minor semiaxis), the porosity, ϕ, is

$$\phi = \frac{n_f}{V}\frac{4}{3}\pi l^3 r , \tag{2}$$

and the ratio of porosity to density

$$\frac{\phi}{\chi} = r . \tag{3}$$

For spherical cavities ($r = 1$), porosity and density are equivalent, but for very flat cracks ($r \ll 1$) we have $\chi \gg \phi$.

Several authors [see Kachanov, 1992 for a review] have developed models relating the change in elastic properties of a solid to the amount of microcraking via a crack density parameter. These theoretical models (based upon the effect of a crack on the elastic properties of an infinite three-dimensional isotropic linear elastic medium) relate the change in bulk elastic properties to the density of cracks, but do not tell us explicitly how crack density actually changes with deformation. For this to be

Correspondence to: J.B. Gómez

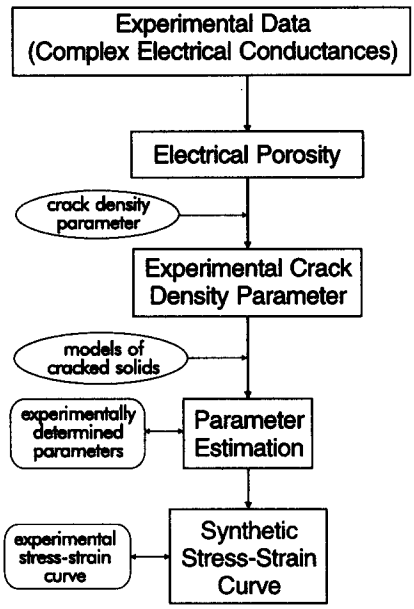

Fig. 1. Flowchart of the inversion procedure. Main steps are depicted as boxes, ellipses refer to theoretical concepts used by the procedure, and rectangles with rounded edges to experimental information used for testing the goodness of the inversion.

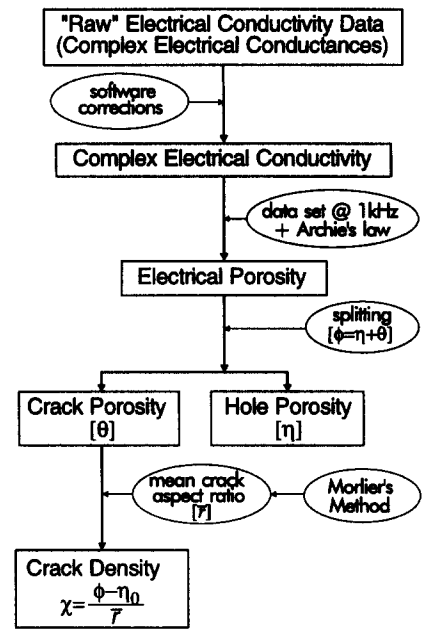

Fig. 2. Flowchart of the main steps involved in the process of converting experimental electrical conductance data into a crack damage parameter, χ.

possible, we need a way of relating crack density to bulk deformation (strain) within the solid. As a direct knowledge of the evolving crack population inside a deforming solid is not possible, we have used electrical conductivity measurements as an indirect measure of the amount of microcracking and, therefore, as a crack density parameter.

The electrical conductivity crack density parameter is then feed into a model of cracked solid to compute the change in effective elastic moduli as deformation procedes. From there, the reconstruction of the stress-strain curve is straightforward. Figure 1 displays a flowchart of the main steps involved in the procedure. As indicated there, and to test the procedure, we have performed a nonlinear fitting to the experimental stress-strain curve, in order to obtain a set of estimated values for the model parameters, which can be then compared with their experimental counterparts. All the tests were made using Darley Dale sandstone, a poorly graded, well cemented, highly porous and permeable arkose. Basic information regarding the tests can be found in Table 1, and further information in the first part of this paper (Glover et al., this volume).

2 Electrical conductivity as a Crack Density Parameter

Figure 2 summarises, again in the form of a flowchart, the steps involved in the conversion of the raw experimental data (complex electrical conductances) into a crack damage parameter. The basic step is the use of Archie's Law,

$$\sigma_r/\sigma_f = \phi^m \tag{4}$$

(where σ_r and σ_f are bulk and pore fluid conductivities, ϕ is porosity, and m Archie's exponent), to obtain *electrical porosity* values from the 1 kHz electrical conductivity data set (see Glover et al., this volume, for a full account of the differences between electrical and volumetric porosity). The resulting electrical porosity can be computed by taking logarithms of (4) and rearranging terms:

$$\phi(\epsilon) = \exp\left[\frac{\ln\sigma_r(\epsilon) - \ln\sigma_f}{-m(\epsilon)}\right], \tag{5}$$

where we have explicitly written the dependence in the axial strain, ϵ, of all the variables.

Equation (5) gives total electrical porosity values. For the definition of a crack damage parameter however, we only need that part of total porosity which is due to the presence of cracks (*crack porosity*). The rest, the porosity due to the presence of equant cavities (*hole porosity*) acts as a background static porosity. Denoting crack

Table 1. Summary of tests performed.

Code	Type	Pore Pressure	Confining Pressure	Porosity
A	Triaxial, undrained	variable	50 MPa	28%
B	Triaxial, undrained	variable	25 MPa	23%
C	Triaxial, drained	atmospheric	50 MPa	16 %

porosity by θ, and hole porosity by η, we can write total porosity as $\phi(\epsilon) = \eta(\epsilon) + \theta(\epsilon)$, and using Eq.(3) to convert crack porosity to crack density we arrive at the following expression for the crack damage parameter, χ,

$$\chi(\epsilon) = \frac{\phi(\epsilon) - \eta(\epsilon)}{\bar{r}} \tag{6}$$

where $\bar{r}$ denotes the initial mean crack aspect ratio of the microcracks.

The behaviour of cracks and holes under a compressive stress field (with or without a pore fluid) is very different [Budiansky and O'Connell, 1976]. Cracks can be closed under 'normal' confining pressures in brittle deformation experiments ($P_{conf} < 0.3$ GPa), but holes will remain open at these pressures. In the pressure range 0-250 MPa, the change in porosity due to the elastic closure of spherical holes is (for a solid with $K_0 = 40$ GPa, $\nu_0 = 0.13$, and $\phi_0 = 15\%$, values compatible with DDS) of the order of 0.1% (Horii and Nemat-Nasser, 1993), much less than the change in crack porosity ($\approx 2\%$) in the same pressure range. We can, therefore, ignore this contribution and consider that all the change in total porosity is due to changes in crack porosity, and take $\eta(\epsilon) = \eta_0$ as a constant during deformation. The expression for the crack damage parameter, equation (6), transforms to

$$\chi(\epsilon) = \frac{\phi(\epsilon) - \eta_0}{\bar{r}} \tag{7}$$

where η_0 is the initial hole porosity (before any deformation takes place). Note, however, that the above consideration is only valid if the rock matrix acts as an elastic continuum where (potentially important) processes like grain sliding and grain rotation are ignored. This extra term in porosity evolution is not modelled with our approach, and is the main responsible of the discrepancy between the toe regions of the synthetic and experimental stress-strain curves (see below and Fig. 3).

3 How the procedure works

The predicted stress, σ_m, acting on a sample submitted to an axial strain ϵ can be written for this model in the general form

$$\sigma_m = f(\epsilon, E_0, \nu_0, \chi) \qquad \chi = f(\eta_0, \bar{r}, \phi)\,, \tag{8}$$

where E_0 is Young's modulus for the crackless (not holeless) solid. The particular form of function f depends basically on four aspects of the model, namely: (i) the *shape* assumed for an individual crack; (ii) the *distribution* of crack orientations; (iii) the presence/absence of a *pore fluid*; and (iv) the way *interactions* among cracks are implemented.

With reference to this last point, we can distinguish three basic group of models of cracked solids: (i) *non-interacting*, where crack interactions are omitted [Walsh, 1965]; (ii) *self-consistent*, where crack interactions are introduced in the model in one step [O'Connell and Budiansky, 1974]; and (iii) *differential*, where crack intreractions are introduced incrementally [Bruner, 1976].

Kachanov [1992] has shown that the approximation of non-interacting cracks may remain accurate at high crack densities for *randomly located* cracks. From computer experiments he showed that the non-interacting approximation provided surprisingly good results well into the domain of strong interactions. Indeed, better results than the differential scheme, both for ramdomly oriented and vertically aligned cracks [see Figs. 8 and 9 in Kachanov, 1992]. Following Kachanov [1992], we will use the non-interacting approximation in our inversion procedure.

Assuming cracks as flat three-dimensional randomly oriented spheroids, the non-interacting approximation gives the following expression for the normalised, effective Young's modulus, E', as a function of crack density [Walsh, 1965]:

$$E' = \frac{E}{E_0} = \frac{1}{1 + g(\nu_0)\chi(\epsilon)}\,, \tag{9}$$

where E is Young's modulus for axial strain is ϵ, and $g(\nu_0)$ is a constant function which depends only on ν_0. For an isotropic solid we have $\sigma_m = E\epsilon$, and using (7) we can rewrite (9) in the final form

$$\sigma_m = \frac{E_0\epsilon}{1 + g(\nu_0)\left(\frac{\phi(\epsilon)-\eta_0}{\bar{r}}\right)}\,. \tag{10}$$

Equation (10) can be interpreted as a synthetic stress-strain ($\sigma_m - \epsilon$) curve. In this equation, ϵ, the axial strain, and $\phi(\epsilon)$, the electrcial porosity as a function of strain are *experimental data*, and E_0, $g(\nu_0)$, ν_0, and $\bar{r}$ are *parameters* which can either be computed through the inversion procedure (nonlinear fitting to the experimental stress-strain curve), or be drawn (at least approximatelly) from other sources or models. The result of the nonlinear fitting is presented in the next section, and the comparison between synthetic and experimental parameter values in the last section.

Table 2. Parameter values for test A.

	Estimated	Experimental
E_0	10.5 GPa	10.9 GPa
ν_0	0.2	0.11-0.25
$\bar{r}$	0.014	0.005-0.02
θ_0	0.02	0.017-0.03

4 Results

We have performed a nonlinear fitting of model equation (10) to the experimental stress-strain curves to obtain an estimate of the model parameters, i.e., E_0, ν_0, η_0, and $\bar{r}$. Figure 3 shows the best-fit synthetic curve for the three tests performed, together with best-fit model parameter values.

We can see from the figure that the inversion procedure works very well up to macroscopic failure (stress-drop point, marked with an open circle on the experimental stress-strain curves), being able to recover both the stress-hardening region located between the end of the straight region and peak stress, and the extended stress-softening region covering the region between peak stress (marked with an open square in Figure 3) and the stress-drop point. Note also, that for *undrained* tests A and B (Figure 3), peak stress and stress-drop points are well apart, but for *drained* test C both points are very close together (This results is a consequence of the stiffening effect that pressurised fluids in the pore space causes on the bulk mechanical properties of the solid during undrained experiments). It is also worth noting that the initial toe region of the experimental stress-strain curve is not reproduced in the synthetic curve due to the fact that we are using a secant Young's modulus.

5 Discussion

How can we test the goodness of the synthetic curves in a more quantitative way than by a simple visual inspection? The answer is performing a *sensitivity analysis* i.e., to change by a certain amount the value of the parameters, one by one, and see how the synthetic stress-strain curves are affected: no change in the curves means very low sensitivity to that particular parameter (i.e., poor constraint on its value); on the other hand, a noticeable change in the inverted curves will mean a high sensitivity of the model to that parameter (i.e., good constraint in its value). Only parameters showing high sensitivity are indeed ' resolved' by the inversion and are, therefore, the only ones that can be properly called ' model parameters'.

We have performed a sensitivity analysis on the four parameters which enter our model: Young's modulus of the crackless solid, E_0, Poisson's ratio of the crackless solid, ν_0, initial crack porosity, θ_0, and initial mean crack aspect ratio, $\bar{r}$. Figure 4 shows the results of the sensitivity analysis. Initial crack porosity was changed

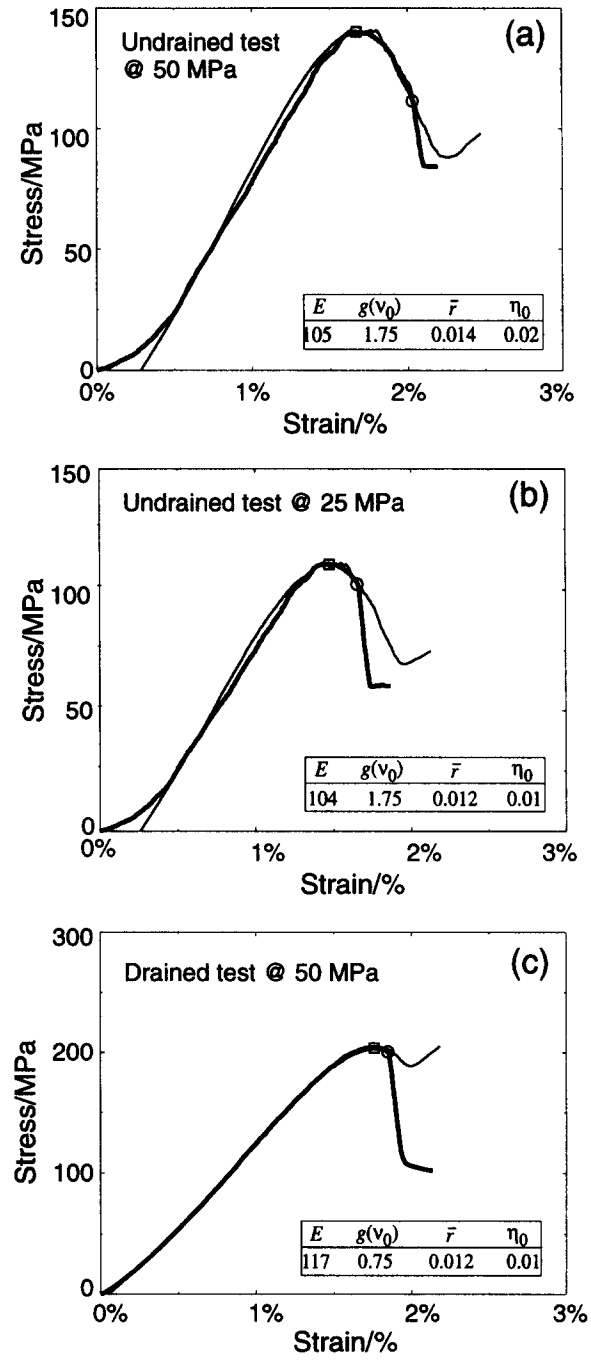

Fig. 3. Best-fit stress-strain synthetic curves after nonlinear fitting to the experimental stress-strain curves. Results are shown for the non-interacting model for the three triaxial tests performed. A: undrained test at 50 MPa confinig pressure; B: undrained test at 25 MPa confinig pressure; C: drained test at 50 MPa confinig pressure. On all the graphs the thick solid line represents the experimental stress-strain curve, and the thin solid line the synthetic curve.

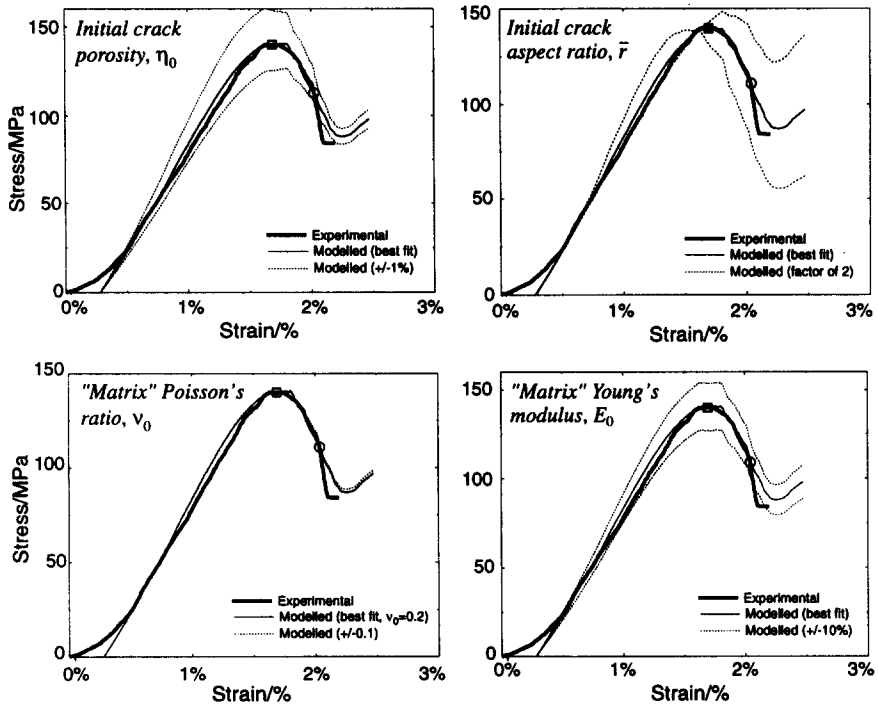

Fig. 4. Sensitivity analysis for test A in Figure 3, again using the non-interacting approximation. On all the graphs the thick solid line represents the experimental stress-strain curve, the thin solid line the synthetic curve, and the two thin dashed lines the synthetic curves after variyng the relevant parameter in the amount shown on the corresponding graph.

in a factor of two around the best-fit value ($\theta_0 = 2\%$); initial mean crack aspect ratio has also been changed in a factor of two (from 0.02 to 0.005, with a best-fit value of around 0.01); initial Poisson's ratio in a factor of two (0.1-0.3, around best-fit value of 0.2); and initial Young's modulus in a +/-10% around its best-fit value of 10.5 GPa.

From the figure we can immediately conclude that Poisson's ratio is a parameter not resolved during the inversion: changing its value in almost the whole possible range for sandstones does not affect the shape of the synthetic curve (This result is quite logical because we are measuring axial quantities, while Poisson's ratio depends also on radial mechanical properties). As for the rest of the parameters, they are well resolved during the inversion and show high sensitivity to changes in their values.

The next step in testing the goodness of the procedure is to compare the best-fit parameter values with experimentally derived values for the same parameters. It is possible to derive initial crack porosity and initial mean crack aspect ratio values from a total porosity against confining pressure curve logged during a hydrostatic deformation experiment [Zimmerman, 1991]. From an exponential fitting to this curve we can obtain directly a value for the *initial crack porosity* (in doing so, we are ignoring the small decrease in porosity due to the elastic closure of spherical cavities; see Glover et al., 1996). The *initial mean crack aspect ratio* can be calculated by means of Morlier's method [Morlier, 1971]. Morlier's method is based upon the fact that low aspect ratio cracks close under lower confining pressures than high aspect ratio cracks. During a hydrostatic deformation experiment, where confining pressure is increased stepwise, changes in total porosity can be adscribed to closure of cracks of increasing initial crack aspect ratio. The output of the method is a crack aspect ratio spectrum (i.e., the probability $P(r)$ of finding a crack of initial crack aspect ratio r), from which it is straightforward to derive a mean crack aspect ratio. Finally, Young's modulus of the crackless solid can be approximated by the slope of the straight part of the experimental stress-strain curve.

Apart from the three triaxial deformation experiments, we have also carried out a hydrostatic test on the same material (DDS) to compute both initial crack porosity and initial mean crack aspect ratio. Table 2 shows the result of the computation, together with the best-fit values obtained from the inversion. The table gathers also the experimental and best-fit value of the other resolved parameter, Young's modulus of the crackless solid. A comparison of both sets of values show that best-fit val-

ues are always bracketed by the experimentally-derived ones, which is an indication that the inversion is able to resolve three parameters that showed high sensitivity during the sensitivity analysis.

6 Conclusions

Measurement of the complex conductivity of saturated rocks during triaxial deformation has the potential for giving useful information concerning the closure and subsequent formation and growth of new cracks.

The sensitivity of complex electrical measurements to crack orientation, and crack connectivity, has been used to create a new direction sensitive crack damage parameter. Stress-strain curves reconstructed using this damage parameter show very good agreement with the measured stress-strain curves.

A nonlinear fit to the experimental stress-strain curves gives a set of best-fit model parameter values which compare very well with experimentally-derived values for these very same parameters. The sensitivity analysis carried out demostrates also that the procedure is able to resolve (i.e shows high sensitivity to) three of the four model parameters (Young's modulus of the crackless rock, initial crack porosity, and initial mean crack aspect ratio), meaning that we can use this procedure to compute important mechanical properties of the deforming solid.

To our knowledge, this is the first time that a mechanical property varying during triaxial deformation has been succesfully modelled using information from the measurement of a transport property.

Acknowledgements. One of the authors (JBG) thanks J.M. Alvarez-Tostado for useful comments and discussions about crack density tensors. This work was funded by NERC research grant GR3/8289 and by Spanish DGICYT grant PB93-0304.

References

Atkinson, B.K. (Ed), *Fracture mechanics of rock*, Academic Press, London, 533 pp., 1987.

Bruner, W.M., Comment on " Seismic velocities in dry and saturated cracked solids", *J. Geophys. Res.*, *81*, 2573-2576, 1976.

Budiansky, B., and O'Connell, R.J., Elastic moduli of cracked solid, *Int. J. Solid Struct.*, *12*, 81-97, 1976.

Glover, P.W.J., Gómez, J.B., Meredith, P.G., Boon, S.A., Sammonds, P.R., and Murrell, S.A.F., Modelling the stress-strain behaviour of saturated rocks undergoing triaxial deformation using complex electrical conductivity measurements, *Surveys in Geophysics*,*17*, 120-144, 1996.

Hill, R., The elastic behaviour of a crystalline aggregate, *Proc. Phys. Soc. London, Ser. A*, *65*, 349-354, 1952.

Kachanov, M., Effective elastic properties of cracked solids: critical review of some basic concepts, *Appl. Mech. Rev.*, *45*, 304-335, 1992.

Lawn, B., *Fracture of brittle solids*, Cambridge Univ. Press, Cambridge, U.K., 375 pp., 1993 (2nd edition).

Morlier, P., Description de l'etát de fissuration d'une roche à partir d'essais non-destructifs simples. *Rock Mechanics*, *3*, 125-138, 1971.

Nemat-Nasser, S., and Horii, M.,*Micromechanics: Overall Properties of Heterogeneous Materials*, North-Holland, Amsterdam, 1993.

O'Connell, R.J., and Budiansky, B., Seismic velocities in dry and saturated cracked solids,*J. Geophys. Res.*, *79*, 5412-5426, 1974.

Walsh, J.B., The Effect of Cracks on the Uniaxial Elastic Compression of Rocks, *J. Geophys. Res.*, *70*, 381-389, 1965.

Zimmerman, R.W., *Compressibility of sandstones*, Elsevier, Amsterdam, 173 pp., 1991.